Hydrodynamics of Turbulent Flows within Arrays of Circular Cylinders

Ana Margarida Ricardo
CEHIDRO-Instituto Superior Técnico, TULisbon, Portugal & Laboratory of Hydraulic Constructions, EPFLausanne, Switzerland. Email: ana.ricardo@ist.utl.pt

ABSTRACT: This article presents a detailed spatial description, employing Particle Image Velocimetry, of a flow within an array of rigid and emergent cylinders with varying density in controlled laboratory conditions. Its main objective is to discuss the spatial distribution of the key terms of the budget of turbulent kinetic energy for different areal number-densities of stems. The following crucial innovations are introduced: a) the flow is quantified from spatial measurements, avoiding the use of the frozen turbulence approximation and b) space-averaging of two-point correlations and statistics is proposed as a means to salvage the formalism of homogeneous-isotropic turbulence. Turbulence characterization follows from second and third-order structure functions, autocorrelation functions, energy spectra and cospectra. Key terms of TKE budget are calculated in the inter-stem space and discussed. For reaches with large mean inter-stem distances equilibrium between production and dissipation is obtained. Turbulent diffusion reveals itself in the interaction of the von Kármán vortex sheet and background turbulence. Convective and pressure diffusion terms are important in the vicinity of individual stems.

KEY WORDS: Turbulence, vegetation, PIV, TKE budget, spatial analysis

1 INTRODUCTION

In the context of environmental sciences, emergent circular cylinders function as an ersatz for wetland vegetation (White and Nepf, 2003, Tanino and Nepf, 2009). The study of the flow in the space among plant stems is highly relevant as its hydrodynamics determine fluxes of suspended sediment, pollutants and nutrients, thus constituting the physical stratum upon which biological and ecological strata are formed (Nepf, 2012). In natural conditions, the flow in the space among plant stems is turbulent provided that the areal distribution of stems is not too dense (quantitative criteria in Sumner et al., 2005). Its spatial heterogeneity is high, mostly determined by the interaction of vortexes shed by individual stems. As a consequence, a complete flow description of the processes occurring at all points in space is difficult to achieve. Upscaling the analysis to spatial scales larger than the mean distance between a stem and its nearest neighbor, namely through the Double-Averaging Method formalism (Raupach and Shaw, 1982, Nikora et al., 2001), has allowed for major progresses in the characterization of stem drag and momentum and scalar fluxes (Raupach et al., 1986, White and Nepf, 2008, Ferreira et al., 2010).

The characterization and quantification of turbulent second moments, namely the turbulent kinetic energy (TKE), is a more challenging problem. For steady flows, the budget of TKE can be written as

$$\underbrace{\frac{1}{2}\overline{u}_j\frac{\partial\overline{u_i'u_i'}}{\partial x_j}}_{\text{I}}+\underbrace{\overline{u_i'u_j'}\frac{\partial\overline{u}_i}{\partial x_j}}_{\text{II}}+\underbrace{\frac{1}{2}\frac{\partial\overline{u_i'u_i'u_j'}}{\partial x_j}}_{\text{III}}=\underbrace{-\frac{1}{\rho}\frac{\partial\overline{p'u_j'}}{\partial x_j}}_{\text{IV}}+\underbrace{2\nu\frac{\partial\overline{s_{ij}u_i'}}{\partial x_j}}_{\text{V}}-\underbrace{\overline{\varepsilon}}_{\text{VI}} \tag{1}$$

where $\overline{u_i}$ stands for time average velocity, u'_i and p' are the fluctuation of velocity and pressure fields, respectively, ν is kinematic viscosity, s_{ij} is the symmetric part of turbulent strain tensor and $\overline{\varepsilon}$ is the dissipation rate of TKE. Overlines stand for the time-average operator. To this date, the spatial distribution of the several terms of equation (1) has not been obtained in laboratory or field experiments and there is no general formulation relating the amount of energy loss to the areal number-density of plant stems and the global Reynolds number. The present work addresses these issues. It draws on two fundamental premises: a) quantification of the TKE budget allows for a deep understanding of the nature of the turbulence and opens possibilities for turbulent modeling (Raupach and Thom, 1981) and b) it is necessary to know in detail the turbulent flow in the inter-stem space before closures to time-averaged or double-averaged conservation equations are attempted.

Following these premises, the main objective of this work is to understand how the convective term, the rate of production, the turbulent diffusion term and the rate of dissipation, respectively terms I, II, III and VI in equation (1), are distributed in the inter-stem space for different areal number-densities of stems. The quantification of these terms is performed in controlled laboratory conditions with Particle Image Velocimetry (PIV).

Three innovations are introduced: i) the very purpose the work, namely a detailed spatial description of the budget of TKE, ii) the experimental procedure, relying mostly on spatial measurements and thus avoiding the use of the frozen turbulence approximation and iii) the theoretical framework for dealing with non-homogeneous flows, employing time and space-averaging as a means to salvage the formalism of homogenous and isotropic turbulence (HIT). The experimental facilities, instrumentation and procedures are discussed in Section 2. The flow is characterized in Section 3 and the theoretical framework is seen in Section 4. Main results are presented and discussed in Section 5. The work is ended by a set of conclusions.

Regarding the symbology used throughout this text, angular brackets $\left(\langle u \rangle\right)$ denote space-average operator while over-lines $\left(\overline{u}\right)$ are used as time-average operator, tildes $\left(\tilde{u}\right)$ represent spatial fluctuations and primes $\left(u'\right)$ time fluctuations. For example $\tilde{u} = u - \langle u \rangle$ and $u' = u - \overline{u}$. The subscript p = 1,2,...,8 are used to identify longitudinal positions while the superscript i = a,b identifies vertical positions.

2 EXPERIMENTAL SETUP AND INSTRUMENTATION

The experimental work was carried out in a 12.5 m long and 40.8 cm wide recirculating tilting flume of the Laboratory of Hydraulics and Environment of Instituto Superior Técnico. The channel has side walls made of glass, enabling flow visualization and laser illumination. The bottom was covered with a horizontal layer of gravel and sand. Arrays of rigid, cylindrical, vertical and emergent stems were randomly placed along a 3.5 m long reach simulating rigid vegetation conditions. The stems, randomly but uniformly distributed, were organized in 15 cm long alternated patches with 1600 stems/m^2 and 400 stems/m^2, separated by 10 cm long transition reaches featuring 5 cm with a density of 1200 stems/m^2 and 5 cm with 800 stems/m^2 (Figure 1). The wavelength of the patchiness is thus 0.5 m. The flow depth was controlled by a coarse gravel weir.

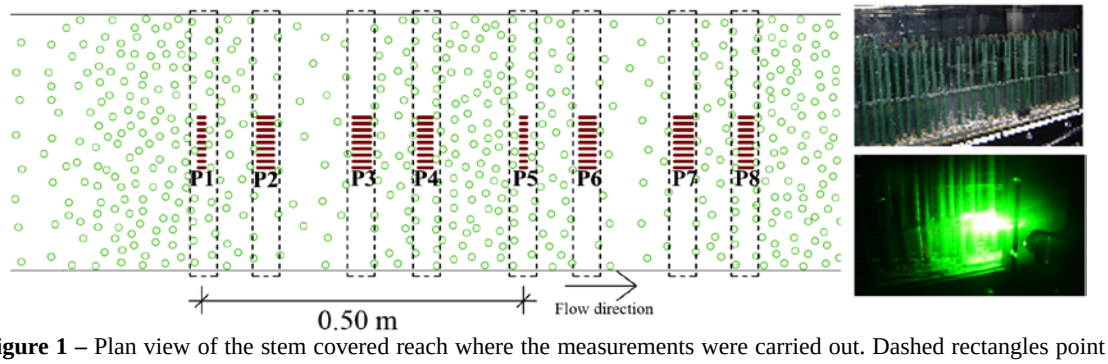

Figure 1 – Plan view of the stem covered reach where the measurements were carried out. Dashed rectangles point out the regions where horizontal maps of velocity were acquired for each longitudinal position, from P1 to P8. The horizontal lines indicate the location of the vertical plans (left). Pictures of the experimental setup (right).

To characterize the flow, 2D horizontal and vertical maps of instantaneous velocity were acquired at eight longitudinal positions (P1 to P8 - Figure 1), covering two patchiness wavelengths. The instantaneous velocity fields were acquired with a 2D Particle Image Velocimetry system (PIV), a technique whose intrusiveness is limited to the introduction of solid targets for flow visualization. The PIV system consisted of an 8-bit 1600 × 1200 px^2 CCD camera and a double-cavity Nd-YAG laser with pulse energy of 30 mJ at wavelength of 532 nm. PIV image pairs were acquired at a frequency of 15 Hz with a time delay of 1500 μs between frames. The targets were polyurethane particles with a mean diameter of 60 μm in a range from 50 to 70 μm and a density of $1.31 g/cm^3$.

Horizontal maps of instantaneous velocity were acquired, at two heights above the bed (Table 1), for each longitudinal position, covering the entire flume width. Maps were approximately 9.5 cm long and 12.5 cm wide, and the spatial resolution yields interrogation volumes of $1.3 \times 1.3 \times 2$ mm^3. For each acquisition 5000 image couples were collected, corresponding to 5.5 minutes of consecutive data. Vertical maps of velocity were acquired in 9 planes for each longitudinal position (Figure 1), with square interrogation areas of 1.5-2 mm. For each plane 10×573 image couples were collected representing a total acquisition time of 6.5 minutes. Vertical data is mainly used to investigate the mean behavior of flow variables through the flow depth at the inter-stem space scale, applying the double averaging methodology (D-AM), as described in Ferreira et al. (2009).

Tests were performed with a discharge of 2.33 ls^{-1}. On Table 1 m represents stem areal number-density, $s = m^{-1/2}$ is the mean inter-stem distance, h is the averaged flow depth, $z^{(i)}$, with i=a,b, is the elevation of the measurement planes, and $Re_p^{(i)} = \left\langle \overline{u}^{(i)} \right\rangle d/\nu^{(i)}$ is the stems Reynolds number, where d=0.011 m is the stem diameter, $\left\langle \overline{u}^{(i)} \right\rangle$ is the double-averaged longitudinal velocity and $\nu^{(i)}$ stands for the kinematic viscosity, which depends on water temperature at the time of the measurements. The presented values are averages of the several spanwise measurements of each longitudinal and vertical positions.

Table 1 - Features of the experimental tests and flow properties for each longitudinal position.

	P1	P2	P3	P4	P5	P6	P7	P8
m (stems/m^2)	1600	800	400	1200	1600	800	400	1200
s (m)	0.025	0.035	0.050	0.029	0.025	0.035	0.050	0.029
h (m)	0.066	0.063	0.062	0.061	0.056	0.054	0.054	0.053
$z^{(a)}/h$ (-)	0.57	0.61	0.61	0.62	0.67	0.69	0.55	0.59
$z^{(b)}/h$ (-)	0.84	0.89	0.90	0.91	0.90	0.93	0.94	0.90
$\left\langle \overline{u}^{(a)} \right\rangle$ (m/s)	0.086	0.093	0.090	0.091	0.092	0.105	0.106	0.100
$\left\langle \overline{u}^{(b)} \right\rangle$ (m/s)	0.091	0.094	0.092	0.092	0.105	0.109	0.104	0.1116
$Re_p^{(a)}$ (-)	1161	1282	1233	1302	1266	1512	1469	1338
$Re_p^{(b)}$ (-)	1281	1268	1242	1301	1473	1533	1462	1564

Throughout this work a Cartesian referential system is considered, where x, y and z correspond to the streamwise, spanwise and vertical directions, respectively, and u, v and w are the corresponding velocity components. However, when evaluating functions evolving increments (correlations or structure functions), one uses longitudinal and transverse coordinates, respectively the axes along the direction of the increments, r, and perpendicular to that direction.

An innovative data analysis technique was employed for the horizontal planes: turbulent velocity series were obtained from subsampling velocity maps in the spanwise direction thus allowing for a larger number of samples in a typical space series for any given instant.

3 FLOW CHARACTERIZATION

Time averaged velocity and vorticity maps, for some longitudinal positions at height $z^{(a)}$, are presented in Figure 2. Velocity maps exhibit heterogeneity at large scales, with alternated low/high velocity regions determined exclusively by the relative distance to the nearest stem. Vorticity maps highlight the quasi-symmetrical pattern of paired vortices shed by each stem, independently of the areal number-density. It should be noted that the mean inter-stem distance ranges from $2.3d$ to $4.5d$ (Table

1), for which two cylinders in tandem would shed vortices in the so-called “reattachment regime” (review in Sumner, 2010). It is thus clear that the vortices are caused by the same mechanism operating in isolated cylinders, unsteady viscous separation forming a von Kármán vortex sheet. Evidently, the space necessary to fully develop the vortex pattern is strongly reduced in the higher stem density (P5), causing the vortexes to look “compressed”, i.e. with little attenuation or diffusion as they travel away from the stem. Conversely, at the lowest stem densities (P6 and P7), vortex strength is seen to decrease, presumably as a result of turbulent diffusion.

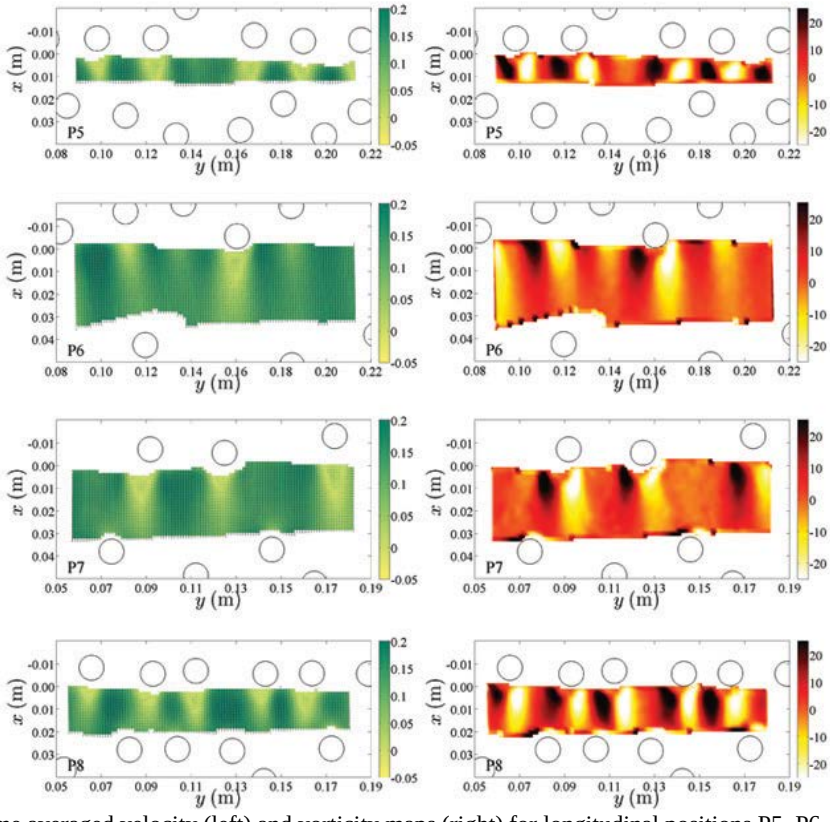

Figure 2 - Time averaged velocity (left) and vorticity maps (right) for longitudinal positions P5, P6, P7 and P8.

It must be emphasized that all stem densities, even at the highest (P5, P8), eddies are allowed to form before interacting with downstream stems (“reattachment”). The main mode of extraction of kinetic energy from the mean flow is wake production, for which the relevant scales are the stem diameter and the mean inter-stem distance. The proper spatial scale of analysis is thus the largest that determines the flow, the inter-stem distance. Spatial series of instantaneous velocities should be twice the inter-stem distance.

These arguments can be better understood if formulated in the spectral space: there are no scales larger than the mean inter-stem distance from which kinetic energy would be extracted directly by the work of drag on stems. There is thus no process adding or subtracting TKE from eddies smaller than the stem diameter and larger than a turbulent microscale. If these scales are sufficiently apart one assumes the existence of an eddy cascade and the quasi-equilibrium hypothesis (Tenekes and Lumley, 1972, Monin and Yaglom, 1975), i.e., that small eddies have been through a sufficiently high number of nonlinear interactions so to lose the anisotropy of energy-containing eddies.

The existence of an eddy cascade is compatible with the power spectra, for longitudinal and transverse velocity components, shown in Figure 3. TKE is extracted from the mean flow at low wavenumbers, with a peak at the vortex shedding frequency (Strouhal numbers slightly depending on the stem density) and is transferred down the cascade at rate $\overline{\varepsilon}$ (reach of $-5/3$ slope as predicted by Kolmogorov 1941 theory).

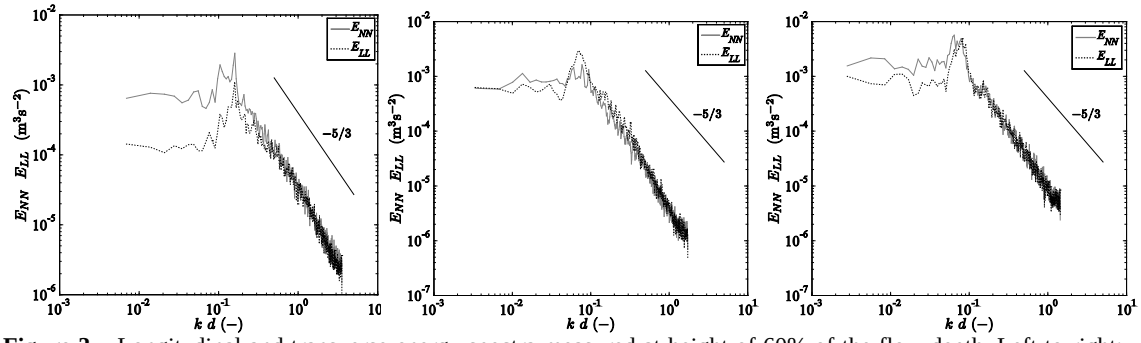

Figure 3 – Longitudinal and transverse **e**nergy spectra measured at height of 60% of the flow depth. Left to right: P5 at y = 24.5 cm; P7 at y = 21.5 cm; P8 at y = 24.0 cm. Data were acquired by Ferreira et al.(2013), with a laser doppler anemometry in identical experimental conditions.

Finally, at high wavenumbers the effect of viscosity is felt and kinetic energy is dissipated into heat ($k = 1/d$ in Figure 3). The hypothesis of isotropy of small scales can be verified by the identity of the longitudinal and transverse spectral functions at high enough wavenumbers ($k > 0.5/d$ for P5 and P8 in Figure 3, more on this issue in the next section).

4 THEORETICAL FRAMEWORK FOR NON-HOMOGENEOUS TURBULENCE

The theory of turbulence is based on statistical analysis of random flow fields. Correlations and moments of the probability distributions are key parameters in characterization of turbulence. Autocorrelation and structure functions are of particular interest.

Figure 4 exemplifies time-averaged transverse autocorrelation functions, R_N, for reaches with the highest and lowest stem density, P5 and P7. These figures show that R_N, present an oscillating behavior around zero, with a wavelength close to s and high amplitude, leading to the conclusion that the mean inter-stem distance, is indeed a key spatial scale to characterize the flow energy budget. Longitudinal autocorrelation functions, R_L, show the same oscillating behavior with smaller amplitude.

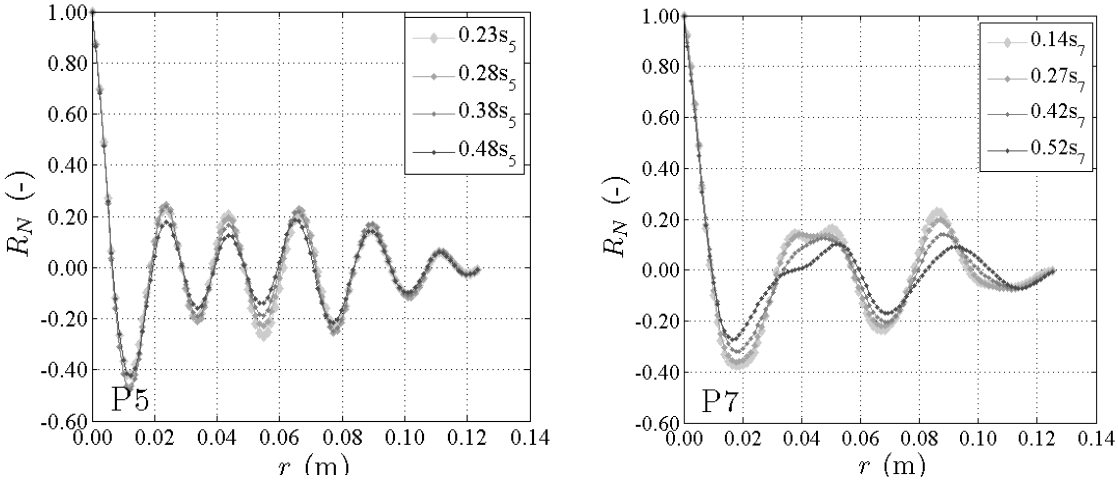

Figure 4 - Transverse autocorrelation function for P5 (left) and P7 (right).

The definition of integral scale based on the integration, between zero and very large r, of the autocorrelation function is, in general, computationally ill-posed for non-homogeneous flows. Herein a macro-scale is defined based on the transverse autocorrelation function, the most sensitive to local flow conditions. The macro-scale, Λ, was defined as the increment r corresponding to the first local maximum of the time and space averaged transverse autocorrelation function, $\langle R_N \rangle$ (Figure 5- left). The average Λ of all the datasets per longitudinal and vertical position are presented on the right hand side of Figure 5.

The values of Λ increase from the highest stem-density patches to the lowest density ones, supporting the idea that the characteristic length scale is correlated with the inter-stem space.

The two point longitudinal, $S_{LL}^{(2)}$, and transverse, $S_{NN}^{(2)}$ second-order structure functions are defined, herein, by $S_{LL}^{(2)}(\alpha+r)=\overline{\left(\tilde{v}(\alpha+r)-\tilde{v}(\alpha)\right)^2}$ and $S_{NN}^{(2)}(\alpha+r)=\overline{\left(\tilde{u}(\alpha+r)-\tilde{u}(\alpha)\right)^2}$, respectively, where r is the increment which has the y-direction, α is any point in the space and $\tilde{v}$ and $\tilde{u}$ are the velocity fluctuations components on the same and the perpendicular direction of the increment, respectively. The overline stands, here, for the appropriate ensemble-average, since the processes are stationary, this may be a time-average. The longitudinal third-order structure function, $S_{LL}^{(3)}$, is defined as $S_{LL}^{(3)}(\alpha+r)=\overline{\left(\tilde{v}(\alpha+r)-\tilde{v}(\alpha)\right)^3}$.

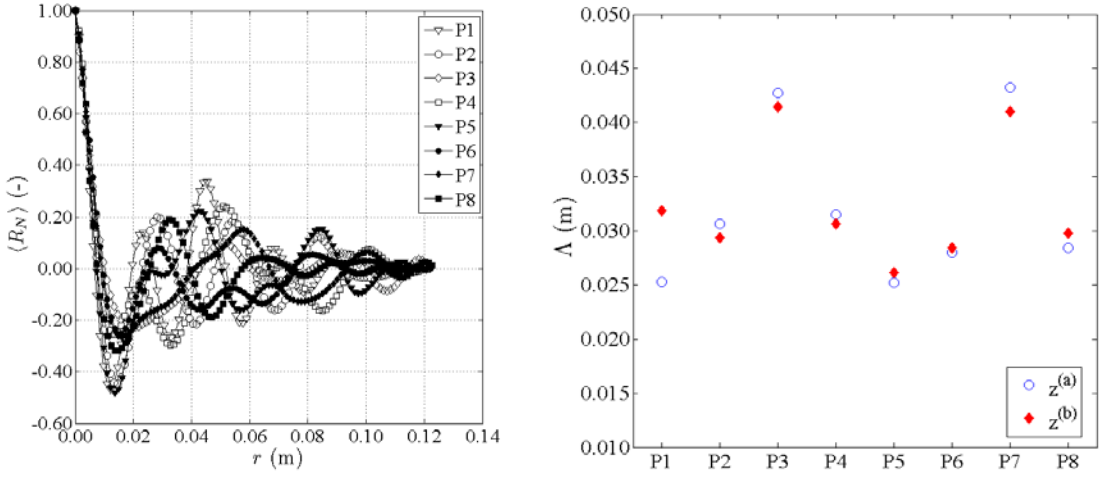

Figure 5 – Double-averaged transverse autocorrelation function for a lateral position at the height $z^{(a)}$ (left) and mean macro-scale for each longitudinal and vertical positions (right).

Since turbulence is not homogeneous, the values of the structure functions depend on the point α and not only on the lag r. If the structure functions are space-averaged, a procedure formally akin to that proposed within the D-AM for the conservation equations, the results $S_{LL}^{(2)}$, $S_{NN}^{(2)}$ and $S_{LL}^{(3)}$ do not depend on any particular α but only on the space lag r: $\left\langle S_{LL}^{(2)}\right\rangle(r)=\left\langle\overline{\left(\tilde{v}(\alpha+r)-\tilde{v}(\alpha)\right)^2}\right\rangle$, $\left\langle S_{NN}^{(2)}\right\rangle(r)=\left\langle\overline{\left(\tilde{u}(\alpha+r)-\tilde{u}(\alpha)\right)^2}\right\rangle$ and $\left\langle S_{LL}^{(3)}\right\rangle(r)=\left\langle\overline{\left(\tilde{v}(\alpha+r)-\tilde{v}(\alpha)\right)^3}\right\rangle$.

Figure 6 shows longitudinal second-order structure functions, $\left\langle S_{LL}^{(2)}\right\rangle$, for the lowest (P3) and the highest (P5) areal number-stem densities. At large scales functions $\left\langle S_{LL}^{(2)}\right\rangle$ and $\left\langle S_{NN}^{(2)}\right\rangle$ reveal an oscillating shape, more pronounced for the case with higher stem density, which expresses the characteristic pattern of high and low velocities associated with the von Kármán vortex sheet. In both longitudinal and transverse functions, there is however a reach of scales, smaller than the macro-scale but not too small, corresponding to the inertial range, where the functions have a 2/3 slope, in accordance to Kolmogorov's 1941 theory. The structure functions are practically similar along streamwise direction.

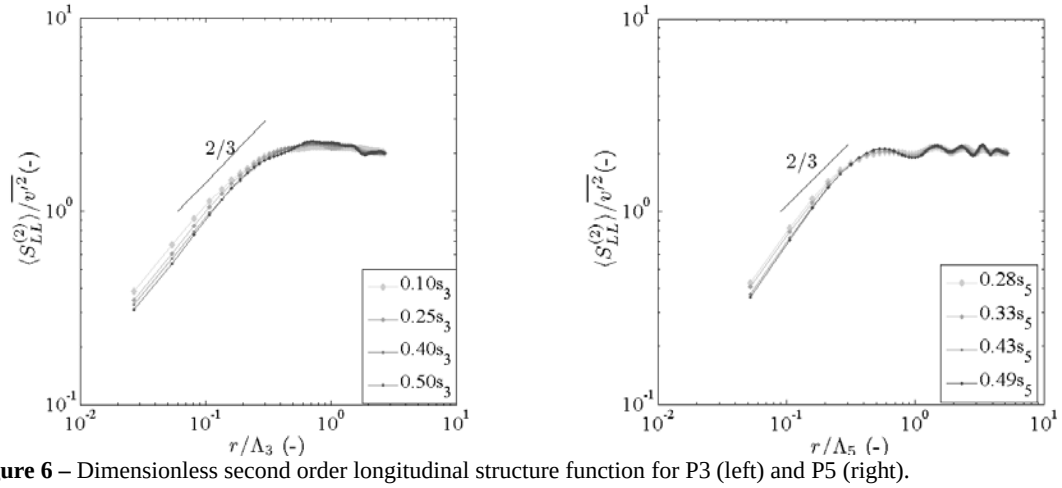

Figure 6 – Dimensionless second order longitudinal structure function for P3 (left) and P5 (right).

Normalized third-order structure functions, for two longitudinal positions, P7 and P5, are presented in Figure 7. The main interest of third-order structures functions is found at small scales, where these are related to energy dissipation rate according to the well-known -4/5 law (Kolmogorov, 1941). On that reach of interest, for all the datasets, we found an essentially linear behavior, roughly coincident with the inertial range identified in the second-order moments. This reach is longer for cases with higher stem density than in the lower density patches.

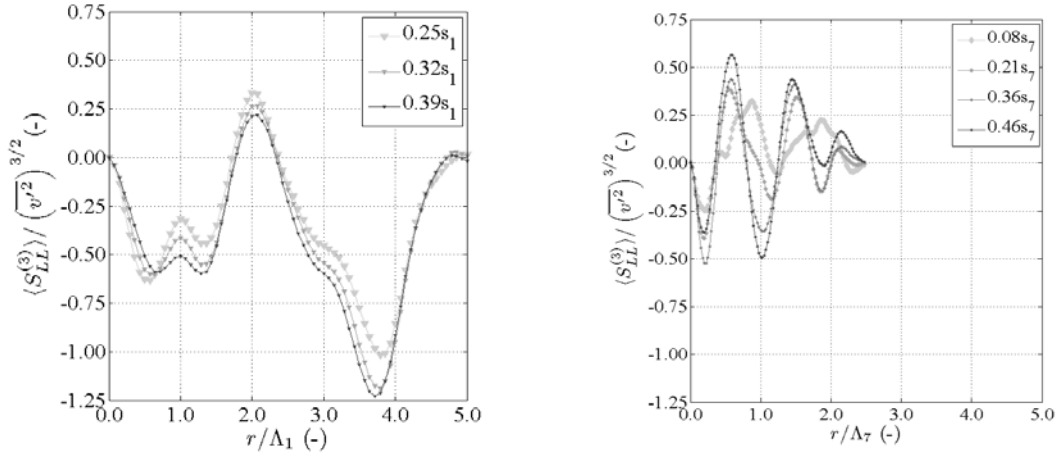

Figure 7 – Third order structure function for P1 (left) and P7 (right).

Motivated by the recent progresses of Double-Averaging Methodologies a new theoretical framework is presented to deal with the non-homogeneity of flows within vegetation. Therefore exploiting the space-averaging of two-point correlations and statistics and following the procedure applied by Monin and Yaglom (1975, pp.120-122) an equation, akin to Kolmogorov's, was derived. Evidently, turbulence remains non-homogeneous but the formalism that led to the relation between second and third-order structure functions in HIT is now applicable rendering similar results:

$$\left\langle S_{LL}^{(3)} \right\rangle (r) = -\frac{4}{5} r \left\langle \overline{\varepsilon} \right\rangle + 6\nu \frac{\partial \left\langle S_{LL}^{(2)} \right\rangle (r)}{\partial r} + I(r) \qquad (2)$$

where ν stands for the kinematic viscosity and $\left\langle \overline{\varepsilon} \right\rangle$ is the mean dissipation rate of energy and $I(r)$ is a function that expresses the effects of large-scale anisotropy and heterogeneity. The detailed deduction of this equation is out of the scope of this paper. However, it should be remarked that function $I(r)$ is

negligible where local isotropy conditions are applicable. Equation (2) shows that any deviations to a linear -4/5 law are attributable to viscous effects and to anisotropy and non-homogeneity. The latter should be relevant only at large scales and negligible at small scales, if local isotropy of the time-averaged flow holds. This hypothesis is evidenced in Figure 3 by the overlap of the longitudinal and transverse energy spectra at large wavenumbers ($E_{LL} \approx E_{NN}$ for $k\,d > 0.5$). Furthermore the local isotropy condition was verified by calculating correlation-coefficient spectrum, $C_{LN}(k) = \left|E_{LN}(x)\right| / \left(E_{LL}(x)E_{NN}(x)\right)^{1/2}$ where E_{LN}(k) is the shear-stress cospectrum and E_{LL}(k) and E_{NN}(k) are the longitudinal and transverse spectra, respectively. Figure 8 shows log-linear plots of correlation-coefficient spectra, C_{LN}, at P7 (low density) and P5 (high density). C_{LN} fall to zero at high wavenumbers ($C_{LN} < 0.05$ for $k\,\Lambda > 5$) proving that within there exists an inertial range of scales where the local isotropy condition is indeed valid. Function $I(r)$ can thus be disregarded for small scales in equation (2).

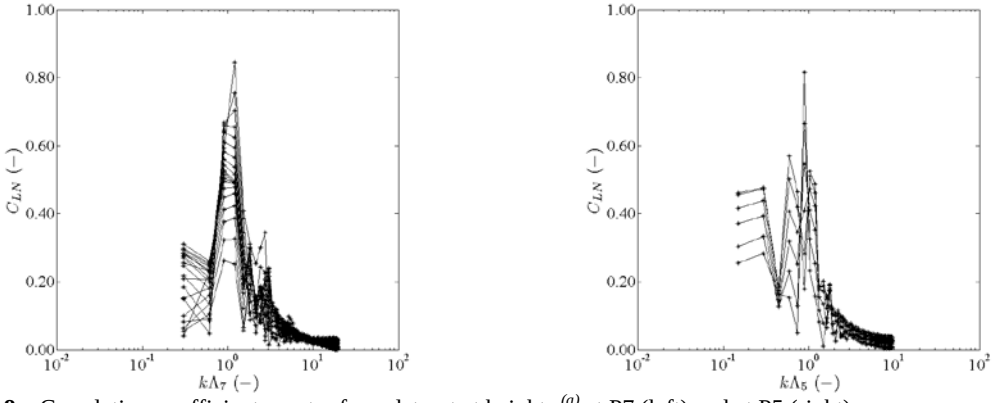

Figure 8 – Correlation-coefficient spectra for a dataset at height $z^{(a)}$ at P7 (left) and at P5 (right).

Summarizing the main consequences of this novel theoretical approach, one finds that flows within arrays of cylinders require heterogeneity and anisotropy but on the large scales identified in the time-averaged field. Considering translations in spanwise direction, the flow is statistically invariant due to the periodic distribution of cylinders (Frisch, 1995, p.73). Since the turbulence of these flows is governed by the inter-stem space, it reveals a strong tendency to isotropy, as verified by the analysis of the correlation-coefficient spectrum (further exploited by Ricardo et al., 2011), allowing for the simplification $I(r) = 0$ at small scales. Assuming enough spatial resolution to include increments within the inertial range of scales and local isotropy in the studied flow, equation (2), with $I(r) = 0$, will be employed to estimate the mean dissipation rate of the flow within arrays of different cylinders densities.

5 RESULTS AND DISCUSSION¨

The dissipation rate was estimated by identifying the first plateau of the compensated version of equation (2), with $I(r) = 0$. Since the second order structure functions may be affected by uncorrelated noise and the noise level is important for small increments, the second term of the previous expression may introduce errors on the estimate of the energy dissipation rate. Therefore the viscous term was applied only at scales where noise was not detected in the corresponding power spectrum. Typically, the noise gets important for scales smaller than 5 mm, which correspond to scales within the linear reach of the third order structure function. Another remark on the estimate of the dissipation rate concerns the definition of the plateau, being considered as valid only if defined by 3 or more points.

The dissipation rate proved to be very sensitive to local conditions once the local arrangement of cylinders strongly impacts its behavior. Figure 9 shows $\langle\overline{\varepsilon}\rangle$ and the sum of productive, diffusive and convective terms of TKE equation (terms I+II+III of equation 1), along streamwise direction for some

datasets, representing also the corresponding local stem distribution. In most of the cases, $\langle \overline{\varepsilon} \rangle$ progresses downstream increasing towards a maximum value and then decreasing (Figure 9a and b), due to the gap without stems where the measurements were carried on. The turbulence generation of each cylinder is felt a bit further downstream, so the initial increasing of $\langle \overline{\varepsilon} \rangle$ reflects the input of the upstream stems.

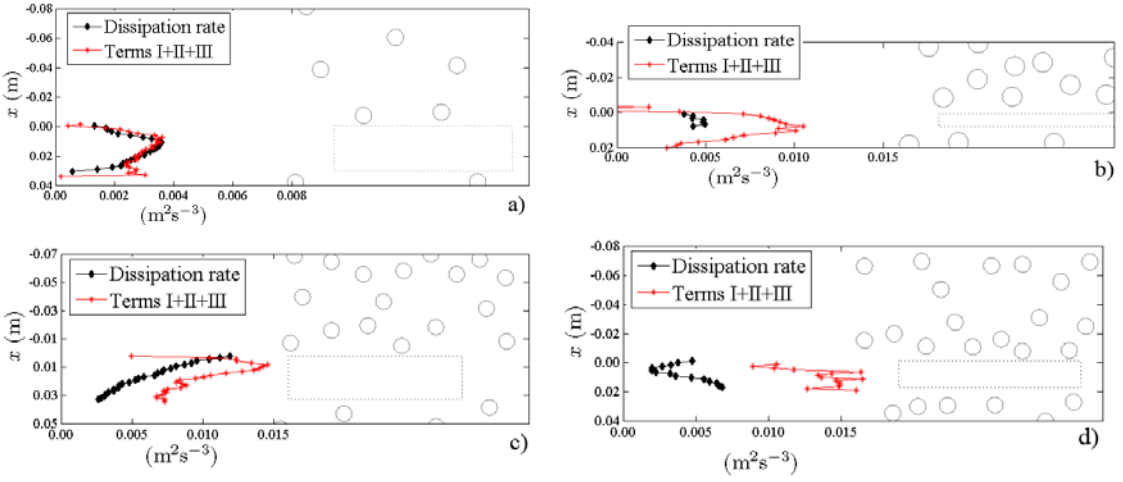

Figure 9 – Balance of productive, diffusive and convective terms (red lines) and dissipation rate of kinetic energy (black lines) along streamwise direction for a dataset at a) P3 ($z^{(b)}$), b) P1 ($z^{(b)}$), c) P6 ($z^{(b)}$) and d) P8 ($z^{(a)}$).

The pattern of decreasing $\langle \overline{\varepsilon} \rangle$ presented in Figure 9c) was found only for P6 in two of the lateral positions at both heights. For this case the relatively low amount of cylinders within the close neighborhood of the measurement reach explains that $\langle \overline{\varepsilon} \rangle$ is already within its decreasing reach. The last case corresponds to a decreasing reach followed by an increasing one, which may be explained by the particularly dense array of stems close to the measured area.

The red lines of the previous graphs represent the average along *y* of the left hand side terms of equation (1). The relative importance of each component of those terms was analyzed leading to the conclusion that components with vertical variations are much smaller than terms with streamwise or spanwise gradients. Moreover, it is believed that $\overline{v'w'} \ll \overline{u'w'}$. Therefore, only the dominant terms were considered, i.e., *x*- and *y*-derivatives and correlations of *u* and *v* components of time averaged velocity or its fluctuations.

Figure 10 shows the variation on the spanwise direction of left hand side of equation (1) for 3 longitudinal positions. One can conclude that magnitude of these energetic terms increases with the stem density as well as with the proximity of the cylinders. These strong spatial oscillations of the turbulent energy fluxes highlight the importance of the von Kármán vortex street on the dynamics of TKE.

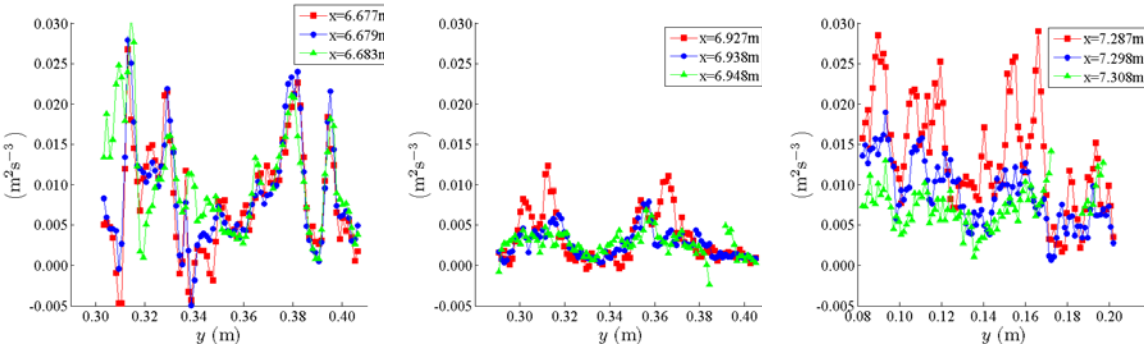

Figure 10 – Balance of the productive, diffusive and convective terms of TKE (II, III and I in equation (1) for 3 "cross-sections" of a dataset. Left to right: P1 (centers of stems at *y* = 0.304, 0.323, 0.343, 0.375 and 0.396 m), P3 (centers of stems at *y* = 0.308 and 0.361 m) and P6 (centers of stems at *y* = 0.082, 0.110, 0.136, 0.160 and 0.184 m).

The sum of terms I, II and III presented in Figure 9 is the average of values for each line, as the ones represented in Figure 10.

In Figure 11 is shown a comparison between terms of TKE herein discussed: production, turbulent diffusion, dissipation and convective term.

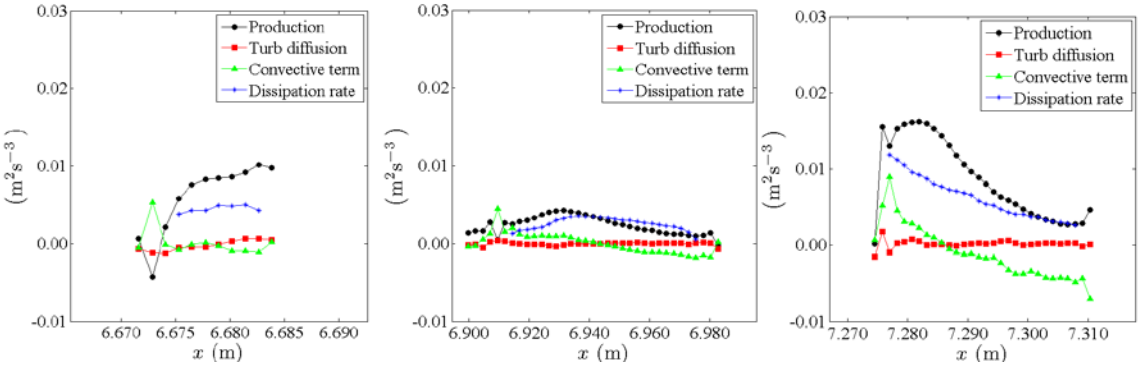

Figure 11 – Average of terms of TKE equation against *x*-coordinate for P1, P3 and P6 (left to right).

Figures 9 and 11 show that the difference between dissipation and the sum of terms I, II and III increases with the density of stems, which is explained by the vortex street of each cylinder and its interaction with the vortex street of neighbor stems. In general, the production increases in the beginning of the measurement reach due to the vortex shedding of the upstream stems. Then, when the mean inter-stem distance is large enough, the productive term decreases towards downstream, following the decrease in the dissipation rate of TKE. The convective term, expressing the interaction of the mean and the turbulent flow field, have an higher importance on the upstream and downstream limits of the measuring area due to the proximity to the array of stems. Turbulent diffusion is, in general, smaller than the other discussed terms, nevertheless it plays an important role mainly due to the presence of the von Kármán vortex streets. It should be noticed that Figure 11 presents averages values of the TKE terms, and as it has been shown on Figure 10, these terms exhibit strong spanwise variations.

Summarizing, downstream of the array of stems all the discussed TKE terms have important magnitudes, so that there is a local disequilibrium between production and dissipation, which decreases towards downstream. Therefore if the inter-stem distance is large enough the equilibrium between production and dissipation terms is reached (Figure 11, P6 and P3). It should also be remarked that pressure and, less likely, viscous terms of equation (1) may also play a non-negligible role in the TKE budget.

An average of the dissipation rate for each longitudinal and vertical position $\langle \overline{\varepsilon} \rangle_l$ was considered. Figure 12a) shows that dissipation rate has a strong correlation with the stem density, since the former increases with increasing density. There is an increase of the dissipation rate from the first to the second wavelength of the array modulation, from P1-P4 to P5-P8, due to the pressure gradient. The figure also presents estimations for dissipation rate based in characteristic scales of velocity and length, defined by $\langle \overline{\varepsilon} \rangle \approx \left\langle \overline{\tilde{v}^2} \right\rangle^{3/2} / \Lambda$, as is commonly used in literature. The graph of $\langle \overline{\varepsilon} \rangle_l$ against Reynolds number based in the macro scale does not show a strong correlation between the two variables. For $z^{(a)}$ the dissipation rate does not change much for a large range of Reynolds number while closer to the free surface similar values of Reynolds number present large differences on the value of $\langle \overline{\varepsilon} \rangle_l$.

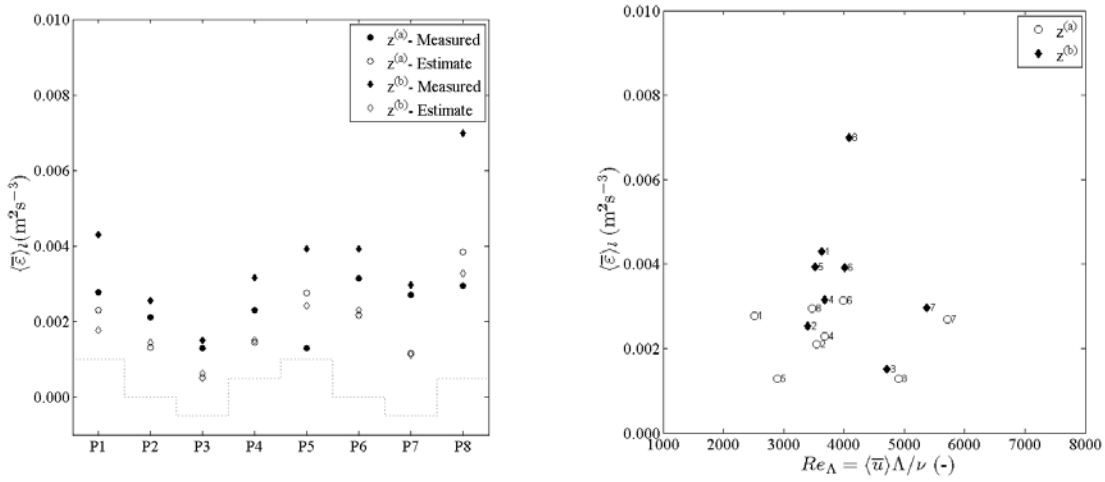

Figure 12 – Measured and estimated mean dissipation rate for each longitudinal position (left) and mean dissipation rate against the macro scale based Reynolds number (right).

6 CONCLUSIONS

The present work, based in detailed 2D PIV measurements, aimed a detailed description of a turbulent flow within an array of emergent stems with varying density. This study brings innovation at the very purpose of the work, the detailed spatial description of the budget of turbulent kinetic energy. Also the experimental procedure is innovative once it is mainly based on spatial measurements which avoid the application of the frozen turbulence approximation. In addition, this work introduces a new theoretical framework to deal with the non-homogeneity of flows within vegetation.

The objective was to discuss the spatial distribution of the key terms of the budget of turbulent kinetic energy for different areal number-densities of stems. It was verified that the flow is turbulent and that turbulence was mainly a result of wake production. Detailed measurements in the inter-stem space revealed that the rate of production has a strong increase above the level of background turbulence associated to the formation of vortices by viscous separation at stems. At sufficient distance from the shedding stems, there is a strong shear rate against which non-negligible Reynolds stresses produce a significant rate of work. Hence, the rate of production has a maximum downstream the last row of shedding stems roughly coincident with the maximum coherence of these vortices. Moving towards downstream, turbulent diffusion contributes to the decrease of the shear rate and hence to the attenuation of the production of TKE. However, this is not seen when inter-stem space is sufficiently small.

Concerning the dissipation rate of energy, an innovative theoretical framework for non-homogeneous flows was presented. Inspired on Double-Averaging methodologies, the proposed framework employs time and space-averaging as means to salvage the formalism of HIT. Being in accordance with the variation of the production of TKE, $\langle \overline{\varepsilon} \rangle$, in general, increases towards a maximum value and then decreases until reaching the next array of stems. Several exceptions to this comportment were found but explained by the local arrangement of the random array of cylinders. When the mean inter-stem distance is large enough, the equilibrium between dissipation and production of TKE is, in general, reached. The space averaged dissipation rate of TKE shows a spatial variation close to the variation of the stem areal number-density. However no strong correlation with the macro scale's Reynolds number was found.

The magnitude of turbulent diffusion is smaller than productive, dissipative and convective terms. Turbulent diffusion is a gradient of the flux of turbulent kinetic energy, therefore its importance is linked to the regions where TKE is itself more important, i.e., on the von Kármán vortex sheet.

The convective terms present higher magnitude close to the stems, both at upstream and downstream limits of measuring reach, where the interaction between the mean and turbulent flow fields is stronger due to flow separation. It has been seen that for large inter-stem distances, there is equilibrium of productive and dissipative terms at sufficient distance from the upstream shedding stems. Therefore

convective terms are balanced by pressure diffusion. This is especially important a downstream end of the measuring reach, just upstream the next row of stems, where a large magnitude of the convective term is associated with the pressure build-up in front of the stems.

The results evidenced a strong dependence on the local arrangement of the array of stems what underlines the importance of a random distribution of the stems per comparison with the patterned based configurations of the stems common in literature. Even when upscaling is envisioned, it is fundamental to understand the behavior of the flow at small scales.

ACKNOWLEDGEMENTS

This study was funded by the Portuguese Foundation for Science and Technology through the projects PTDC/ECM/099752/2008 and PTDC/ECM/11760/2010 and the grant SFRH/BD 33668/2009.

References

Ferreira, R. L., Ferreira, L. M., Ricardo, A. M. and Franca, M. J., 2010. Impacts of sand transport on flow variables and dissolved oxygen in gravel-bed streams suitable salmonid spawning, River Res. Applications, 26, 414–438

Ferreira, R. M. L., Ricardo, A. M., and Franca, M. J., 2009. Discussion of 'Laboratory investigation of mean drag in a random array of rigid, emergent cylinders' by Heydi M. Nepf and Yukie Tanino, Journal of Hydraulic Engineering, vol. 134, no 1, 2008," Journal of Hydraulic Engineering 135, 690–693.

Ferreira, R. M. L., Ricardo, A. M., and Koll, K., 2013. Experimental Characterization of the TKE Budget in Flows with Emergent Vegetation, Proceedings 35th IAHR World Congress, Chengdu, China.

Frisch, U., 1995. Turbulence. The legacy of A. N. Kolmogorov. Cambridge University Press, Cambridge, UK.

Monin, A. S. and Yaglom, A. M.,1975. Statistical Fluid Mechanics: Mechanics of Turbulence, edited by J. Lumley, Vol. II, MIT Press, Boston, USA.

Nepf, H., 2012. Flow and transport in regions with aquatic vegetation, Ann. Rev. of Fluid Mechanics 44, 123–142.

Nikora, V., Goring, D., McEwan, I., and Griffiths, G., 2001. Spatially averaged open-channel flow over rough bed, Journal of Hydraulic Engineering 127, 123–133.

Raupach, M. R., Coppin, P. A., and Legg, B. J., 1986. Experiments on scalar dispersion within a model plant canopy - part i: turbulence structure, Boundary Layer Meteorology 35, 21–52.

Raupach, M. R. and Shaw, R. H., 1982. Averaging procedures for flow within vegetation canopies, Boundary-Layer Meteorology 22, 79–90.

Raupach, M. R. and Thom, A.S., 1981. Turbulence in and above plant canopies, Ann. Rev. Fluid Mech, 13, 97-129.

Ricardo, A. M., Franca, M. J., and Ferreira, R., 2011. Anisotropic turbulent flow in flows within emergent rigid vegetation, in Geophysical Research Abstracts, Vol. 13, EGU 2011-1294-1, EGU General Assembly, Vienna.

Sumner, D., 2010. Two circular cylinders in cross-flow: A review, Journal of Fluids and Structures, 26, 849-899

Sumner, D., Richards, M. and Akosile, O., 2005. Two staggered circular cylinders of equal diameter in cross-flow, Journal of Fluids and Structures, 20, 255 - 276

Tanino, Y. and Nepf, H. M., 2009. Laboratory investigation of lateral dispersion within dense arrays of randomly distributed cylinders at transitional Reynolds number, Physics of Fluids 21, 046603: 1–10.

Tenneles, H. and Lumley, J., 1972. A first course in turbulence, The MIT press.

White, B. L. and Nepf, H. M., 2003. Scalar transport in random cylinder arrays at moderate Reynolds number, Journal of Fluid Mechanics 487, 43–79.

White, B. L. and Nepf, H. M., 2008. A vortex-based model of velocity and shear stress in a partially vegetated shallow channel, Water Resources Research 44, WR005651.